PHYSICAL REVIEW B **85**, 094109 (2012)

Electron dynamics of shocked polyethylene crystal

Patrick L. Theofanis, Andres Jaramillo-Botero,* and William A. Goddard III†
California Institute of Technology, Division of Chemistry and Chemical Engineering, 1200 E. California Boulevard, Pasadena, California 91125, USA

Thomas R. Mattsson and Aidan P. Thompson
Sandia National Laboratories, Albuquerque, New Mexico 87185, USA
(Received 12 January 2012; published 22 March 2012)

Electron force field (eFF) wave-packet molecular-dynamics simulations of the single shock Hugoniot are reported for a crystalline polyethylene (PE) model. The eFF results are in good agreement with previous density-functional theories and experimental data, which are available up to 80 GPa. We predict shock Hugoniots for PE up to 350 GPa. In addition, we analyze the structural transformations that occur due to heating. Our analysis includes ionization fraction, molecular decomposition, and electrical conductivity during isotropic compression. We find that above a compression of 2.4 g/cm^3, the PE structure transforms into an atomic fluid, leading to a sharp increase in electron ionization and a significant increase in system conductivity. eFF accurately reproduces shock pressures and temperatures for PE along the single shock Hugoniot.

DOI: 10.1103/PhysRevB.85.094109 PACS number(s): 82.35.Lr

I. INTRODUCTION

The material response of polyethylene (PE) to shock and its behavior in the warm dense matter (WDM) regime is important because it is a common ablator material in direct-drive inertial confinement fusion (ICF) experiments.[1,2] Experiments at the National Ignition Facility (NIF) have demonstrated that the ICF burn efficiency can be non-negligibly impacted by the capsule material, so it is crucial to understand the properties of this material.[2,3] Macroscopic modeling of capsule materials for these experiments requires accurate constitutive engineering material models. Producing quality engineering models requires a detailed microscopic understanding of the equations of state (EOS), electrical conductivity, and optical properties for a given material. Here, we examine the effects of electronic excitations during hydrostatic shock of PE.

Theoretical studies of PE in extreme conditions are abundant. A variety of methods including quantum mechanics (QM), conventional force fields, and reactive force fields are able to reproduce a common equation of state gauge: the experimental Rankine-Hugoniot curve.[1,4] Born-Oppenheimer quantum molecular-dynamics (BOQMD) methods and conventional force fields presume adiabaticity in their approach to simulating the high-energy states of PE. This assumption limits the scope of these techniques to temperatures well below the Fermi temperature, near the electronic ground state of PE.[5] Conventional and reactive force fields are parametrized based on Born-Oppenheimer potential energy surfaces. The result of using Born-Oppenheimer methods is that the effects of electronic excitations are absent from the system's EOS, and along the particular EOS path corresponding to the Rankine-Hugoniot. Quantum-mechanical finite-temperature density-functional theory (DFT) methods, unlike BOQMD approaches, allow for electron excitations, however the Kohn-Sham orbital description precludes these methods from revealing dynamic electron effects such as Auger processes.[6,7] Finite-temperature DFT methods, like those used in Refs. 4 and 1, are good points of comparison for the electron force field (eFF) because they allow for thermal electron excitations.

II. THE ELECTRON FORCE FIELD

The first-principles-based electron force field is a mixed quantum-classical approach for studying nonadiabatic reactive dynamics based on floating spherical Gaussian wave packets.[8] In the past, eFF was successfully applied to nonadiabatic processes such as Auger decay,[9] H_2 in the WDM regime,[10] the hydrostatic[11] and dynamic[12] shock Hugoniot, and exo-electron emission due to fracture in silicon.[13] eFF is unique in that electronic and nuclear degrees of freedom are separate, which allows for nonadiabatic motion to occur naturally. eFF is many orders of magnitude faster than QM, which allows us to perform large-scale and long-time-scale dynamics simulations.[12]

The eFF method provides an approximate description of quantum dynamics by describing every electron as a floating spherical Gaussian orbital whose position and size vary dynamically while the nuclei are treated as classical point-charge particles.[14] Here the total N-electron wave function is written as a Hartree product of one-electron orbitals (rather than as an antisymmetrized product). Orthogonality resulting from the Pauli principle is enforced with a spin-dependent Pauli repulsion Hamiltonian that is a function of the sizes and separations of these Gaussian orbitals. The Pauli potential accounts for the kinetic energy change due to orthogonalization, arising from the Pauli principle (antisymmetrization).[8,15] An additional quantum-derived term in the eFF Hamiltonian is the kinetic energy for each orbital, which accounts for the Heisenberg principle. The full Hamiltonian in eFF also incorporates classical electrostatic terms between nuclei or electrons.

eFF energies and forces are used to propagate the nuclei and electron wave function in time using semiclassical wave-packet molecular dynamics.[16] The Gaussian wave packets are subject to the potential produced by neighboring nuclei and electrons; this potential is anharmonic, so the size of each Gaussian is stable at low and intermediate energies. The fact that the wave packets are stable is vindication of the harmonic assumption made during the derivation of the wave-packet

translational and radial equations of motion.[8,12,16] If an electron is excited sufficiently, it may escape its local potential and its radius may expand, causing the collapse of the wave function; this is the eFF analog of electron delocalization. A radial restraint is used to prevent excited electrons from expanding infinitely (which would lead to infinite kinetic energy): $E_{\text{res}} = 1/2k_s(s - L_{\text{min}}/2)^2$ for $s > L_{\text{min}}/2$, where L_{min} is the smallest box bound and s is the Gaussian radius. k_s is arbitrarily set to 1 hartree per bohr, and the resulting force is $F_{\text{res}} = -k_s(s - L_{\text{min}}/2)$. The conditions that invoke this restraint were not encountered in our simulations, though had they been, the effect on the validity of the simulation would be minimal. A large electron imparts a force on those electrons and nuclei that it overlaps with, which is manifested in an increase in pressure. Invoking the radial restraint limits the increase in pressure and kinetic energy.

For this study we used a parallel version of eFF which is included in the LAMMPS software package.[12,17] The LAMMPS website provides performance comparisons of eFF and other conventional and reactive force fields.[18] eFF is roughly 300 times slower (cpu time per time step per particle) than a conventional Lennard-Jones potential, yet it has been demonstrated to have linear strong and weak scaling over a broad range of system sizes and number of processors in LAMMPS. It is important to note that electrons are explicitly described in eFF, i.e., it takes one carbon, two hydrogen, and eight electrons to describe a single CH_2 unit. Consequently, using the true electron mass in eFF requires the use of much shorter integration time steps, on the order of attoseconds.

III. COMPUTATIONAL DETAILS

A crystalline PE model was created by truncating and hydrogen passivating the chains in a $2 \times 6 \times 3$ supercell of orthorhombic polyethylene. Truncating the chains in this fashion prevents unnatural stresses from forming along the length of each chain. The final cell contained 12 $C_{12}H_{26}$ molecules: 1632 particles total, 144 carbon, 312 hydrogen, and 1176 electrons. In real samples of crystalline PE, the chains are finite in length and the PE is only crystalline in small domains with lamella ranging from 70 to 300 Å in thickness and extending several microns laterally.[19,20] Because eFF lacks van der Waals forces, the equilibrium volume of crystalline PE is 30% too large in eFF. To counter this, the volume of the PE cell was adjusted so that the ground-state reference has a density of 0.95 g/cm^3; this produced 1.3 GPa of stress, which was subtracted from all subsequent pressure computations. To generate points along the Hugoniot path, we prepared samples of increasing density up to 3.0 g/cm^3 by isothermally and isotropically compressing the reference cell at 300 K. The temperature was controlled with a Nosé-Hoover thermostat so that the temperature, number of particles, and volume (NVT) were defined. Each cell was then ramped to 1500 K over the course of 500 fs and it was allowed to equilibrate as a microcanonical ensemble with a fixed energy, volume, and number of particles (NVE) at 1500 K for another 500 fs. After heating, each cell was cooled by decreasing the temperature in 30 K steps during which 200 fs of NVT dynamics was followed by 200 fs of NVE dynamics.

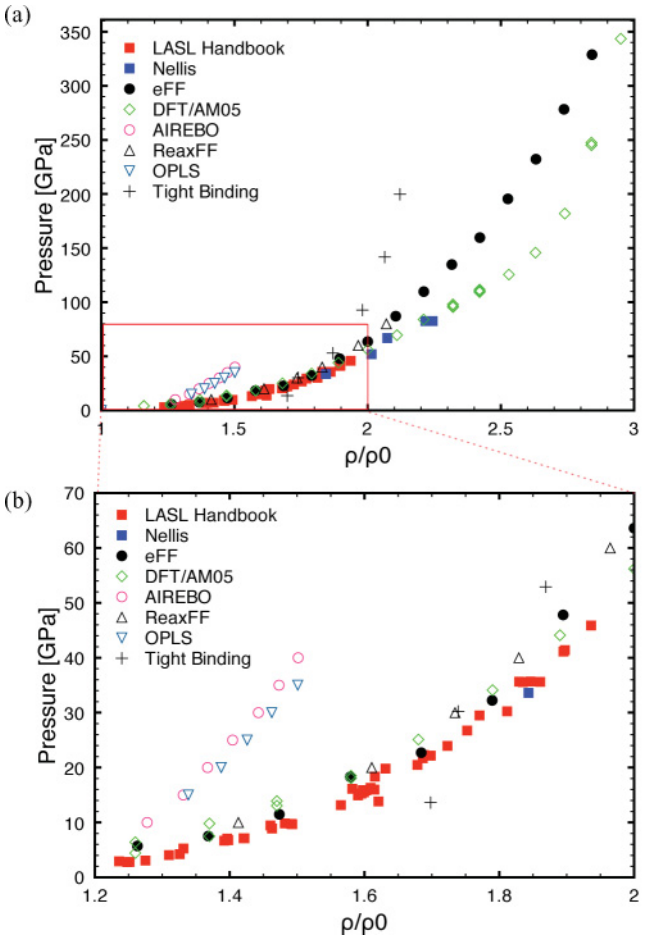

FIG. 1. (Color online) (a) The principal Rankine-Hugoniot for PE. Experimental data from the LASL shock compression handbook[24] and Nellis[25] are provided along with data for the classical MD potentials (OPLS and AIREBO).[4] A reactive force field (ReaxFF[4]) and quantum-mechanical approaches (DFT/AM05 and tight binding[26]) are included for comparison. (b) An expansion of the low compression region of the Hugoniot .

In the eFF method, the electron mass is defined in three separate locations: (i) in the electronic kinetic energy (i.e., wave function), (ii) in the spin-dependent Pauli energy, and (iii) in the equations of motion.[8,12] The effect of modifying the electron mass in (i) and (ii) affects the sizes of electrons in atoms and the lengths of bonds in molecules, therefore we keep these fixed to avoid disrupting the chemistry of the system. In all potential energy terms, the electron mass is set to the true electron mass (5.486×10^{-4} amu). However, the user may define a different *dynamic electron mass* to evolve the kinetic equations of motion.[8,12] Changing the mass in the equations of motion varies the overall time scale of excited electron motions, with the time scale of excitation relaxations and energy transfer proportional to $\sqrt{m_e}$. We refer to this as changing the dynamic masses. This does not affect the net partitioning of energy in the system nor the magnitude of the thermodynamic parameters we are interested in measuring. This does not alter the system's chemistry, just its evolution in time. We verified this by computing a few Hugoniot points with 1.0, 0.1, and 0.01 amu dynamic mass and found negligible differences in pressure and temperature at these points. An

artificially heavy electron mass enables the use of longer integration time steps. For this study, we set the dynamic electron mass to 0.1 amu. To conserve mass in the system, we subtracted the mass of each atom's electrons from the standard atomic mass (e.g., we set carbon atom masses to 11.4107 amu and hydrogen atom masses to 0.907 94 amu). With this dynamic electron mass, we used an integration time step of 0.5 attoseconds (0.0005 fs).

The temperature in eFF (like pressure) is extracted from the dynamics simulation using classical virial expressions summing the kinetic energies of all the nuclear and electronic degrees of freedom:

$$E_{\mathrm{ke}} = \tfrac{3}{2} N k_B T. \tag{1}$$

The kinetic contribution to the heat capacity is set to $\frac{3}{2}k_B$ by setting N to the number of nuclei, which is valid for temperatures well below the Fermi temperature. The temperatures presented in this paper were computed using Eq. (1).

A Hugoniot curve is the locus of thermodynamic states that can be reached by shock compression of a specific initial state. These states satisfy the Rankine-Hugoniot energy condition[21,22]

$$U - U_0 = \tfrac{1}{2}(P + P_0)(V_0 - V), \tag{2}$$

where U is the internal energy, P is the pressure of the system, and V is the cell volume. It is assumed that each point along this curve corresponds to a state of thermodynamic equilibrium wherein the stress state is hydrostatic. For solids, this latter condition is only valid when the yield stress is much lower than the mean stress.[23] When the initial-state variables P_0, V_0, and U_0 are those of the uncompressed sample at room temperature, the Rankine-Hugoniot curve is called the principal Hugoniot. We generated states on the principal Hugoniot using the following iterative procedure. First the volume of the system is specified, representing a particular degree of compression. How each density point was prepared is described in the preceding paragraph. The temperature of the system is quickly increased by changing the set point of the thermostat. A total of 100 fs of dynamics are run after the thermostat jump, during which averages of the energy, temperature, and pressure of the new state are obtained. These values are used to evaluate the residual energy for a time step i, $E_{\mathrm{res},i}$, given by

$$E_{\mathrm{res},i} = (U - U_0) - \tfrac{1}{2}(P + P_0)(V_0 - V). \tag{3}$$

When $|E_{\mathrm{res},i}|/E_{\mathrm{ke},i} < 0.05$, the Hugoniot condition is considered satisfied. If this inequality is not satisfied, an additional 100 fs iteration is performed. The new thermostat set point is calculated from

$$T_{i+1} = T_i\left(1 - 0.05\frac{E_{\mathrm{res},i}}{E_{\mathrm{ke},i}}\right), \tag{4}$$

where $E_{\mathrm{ke},i}$ is the average kinetic energy of the system at step i. Once this iterative procedure has converged, the thermostat is turned off and the system is allowed to evolve for an additional 3 ps. This calculation ensures that the Hugoniot condition is actually met and the properties of the systems were obtained from these dynamics.

IV. RESULTS AND DISCUSSION

A. The principal Hugoniot

Figure 1 is the principal Hugoniot projected onto the pressure-density plane. For densities below 2.0 g/cm^3, eFF matched the experimental and DFT Hugoniot points quite closely [see Fig. 1(b)]. At higher densities, the eFF simulations overpredicted the shock pressure relative to DFT. Above 2.0 g/cm^3, the results show that eFF is systematically "stiffer" than the experimental and DFT/AM05 (Ref. 27) data. However, eFF provides better agreement with the experimental Hugoniot points than typical classical MD potentials such as AIREBO,[28] OPLS,[29] and exp-6 (not shown);[30] the data for these can be found in Ref. 4. eFF also outperformed the tight-binding QM method above 2.0 g/cm^3. These results demonstrate the difficulty in modeling the behavior of materials under shock compression. Figure 2 shows the temperature-pressure plane

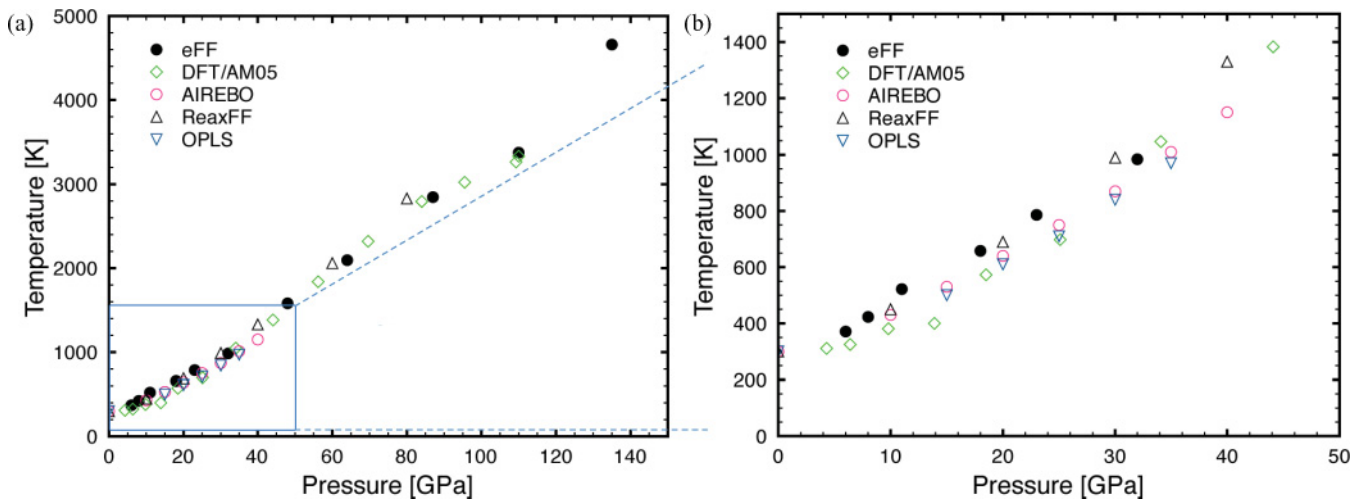

FIG. 2. (Color online) (a) The pressure-temperature locus of the Hugoniot curve for the eFF, DFT/AM05, OPLS, AIREBO, and ReaxFF methods. (b) An expansion of the pressure-temperature seam for lower pressures.

of the Hugoniot calculated by the methods in Fig. 1 for which temperature data were available. The system temperatures produced by the eFF calculations are in good agreement with conventional force fields, reactive force fields, and QM.

At high compression, interesting material features appear in the principal Hugoniot. In the AM05 data series, a shoulder feature appears at 2.3 g/cm^3. This feature is not as pronounced in the eFF Hugoniot; however, for both methods, inflections in the temperature-density plane of the Hugoniot curve indicate structural transitions (see figure 1 of the supplemental material). Subtle temperature suppression is evident in the eFF temperature-density curve at 2.0 and 2.6 g/cm^3. These data features correspond to tangible transitions in the molecular structure. Mattsson reported that the AM05 shoulder at 2.3 g/cm^3 corresponded to PE backbone bond breaking.[4] The causes for the eFF data features will be discussed shortly.

B. Structural decomposition

An analysis of the pairwise radial distribution functions (RDFs) for different degrees of compression demonstrates that significant structural decomposition occurs upon shock.[31] Figure 3(a) shows that carbon bonds are compressed as the sample is compressed. As the density of the material increases, the nearest-neighbor C-C pair peak (1.55 Å) broadens and the next-nearest-neighbor C-C pair distance (2.6 Å) is lost, indicating that the carbon backbone is fragmented. The C-H pair distribution function in Fig. 3(b) also demonstrates that tetrahedral order is lost due to shock compression. The H-H pair distribution function in Fig. 3(c) also shows that geminal (normally 1.95 Å), synclinal (2.4 Å), and antiperiplanar (3.2 Å) nearest-neighbor hydrogen peaks are lost at high compression. The 2.9 g/cm^3 series resembles a classical Lennard-Jones fluid. For densities between 2.0 and 2.1 g/cm^3 corresponding to temperatures around 3000 K, small peaks in the H-H data in Fig. 3(c) near 0.7 Å reveal the formation of molecular hydrogen. Mattsson and collaborators also found H_2 formation when their shocked PE reached 2800–3100 K.[32] In their simulations and in the eFF simulations, this temperature range corresponded to densities of 2.2–2.3 g/cm^3. Select pair correlation functions near DFT/AM05 Hugoniot points are available in the supplemental material. For temperatures higher than 3100 K, the molecular hydrogen dissociates, while at lower temperatures the hydrogen atoms do not have enough energy to dissociate from the polyethylene backbones. At high degrees of compression (>2.2 g/cm^3), the RDFs collectively reveal a fluid phase. The eFF results are consistent with MD and DFT results for equivalent temperatures.

One of eFF's greatest assets is its ability to separate electron degrees of freedom, energies, positions, momentum, and forces from those of the nuclei. This gives us an unrivaled ability to measure electronic physical quantities. In our investigation of PE, we have used this to measure the ion fraction at each stage of shock. To do this, we measure the kinetic and potential energy of each electron at each time step in our simulations.

Figure 4 shows the onset of electron ionization at 2.5 g/cm^3. Ionization increases exponentially for higher densities. The rapid increase in the ionization fraction above 2.6 g/cm^3 is evidently the cause of the shoulder in the temperature-density

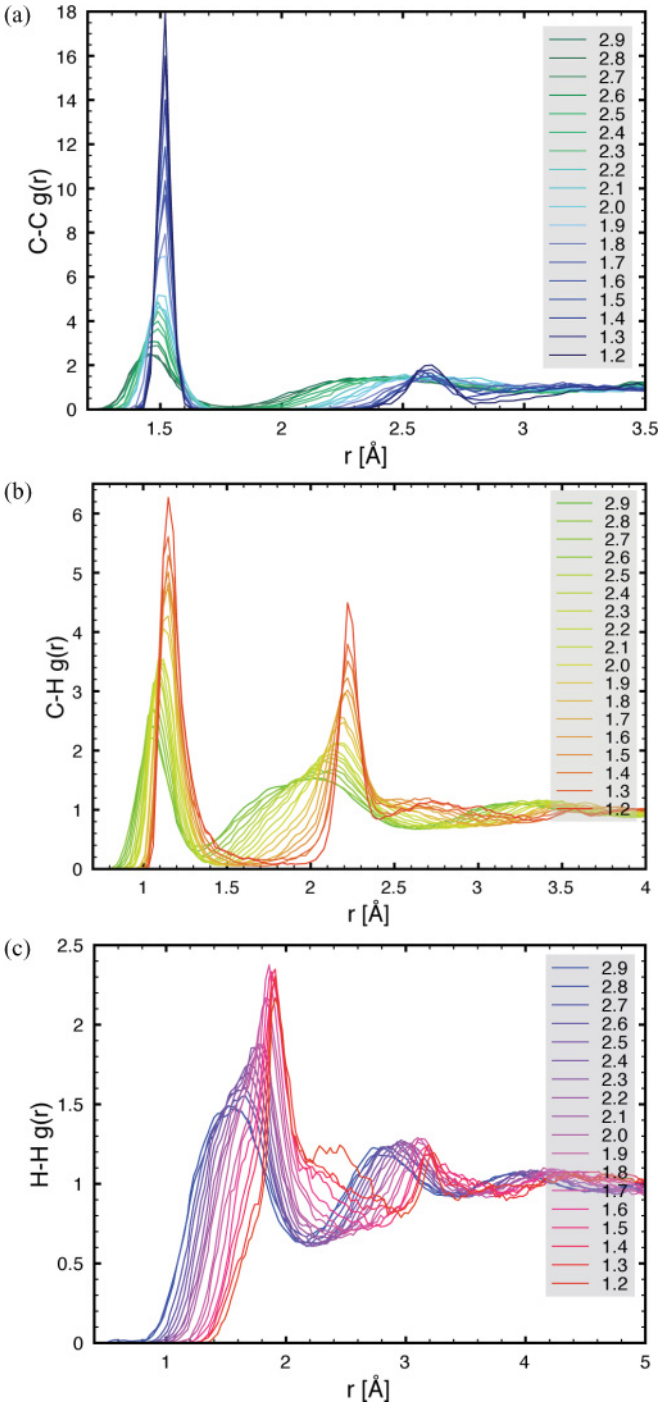

FIG. 3. (Color online) Radial distribution functions for (a) C-C atom pairs, (b) C-H pairs, and (c) H-H pairs. Each curve corresponds to a different density point (g/cm^3) defined by the colors in the legend.

Hugoniot between 2.6 and 2.7 g/cm^3. Above this threshold, electron ionization draws energy from the system and this affects the pressure and temperature of the Hugoniot. The production of carriers in our simulations implies that PE is conductive at high states of compression. The production of ions is precipitated by the breaking of C-C bonds, and this relationship is evident in Fig. 4. The percentage of intact backbone for the DFT/AM05 study is also presented in Fig. 4. eFF predicts that the polymer backbone begins to fracture at

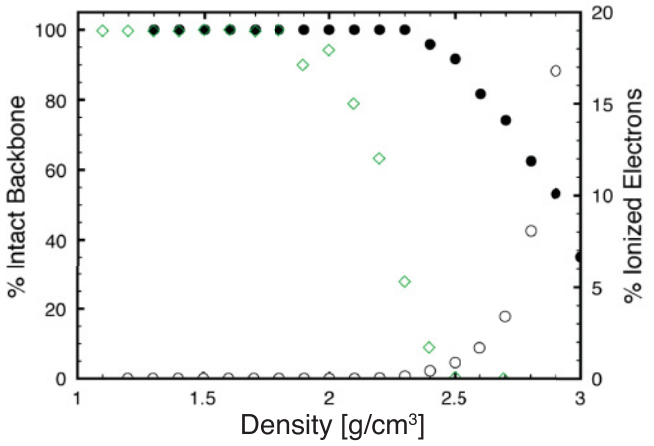

FIG. 4. (Color online) Structural decomposition along the PE Hugoniot. The circles correspond to the % intact C-C backbone for the eFF simulations. The open diamonds show the results from DFT/AM05. The secondary axis shows the % ionization along the Hugoniot calculated from the eFF simulations in open circles.

2.4 g/cm^3 and DFT/AM05 predicts that fracture begins at 2.0 g/cm^3.

Curiously, both the DFT/AM05 and eFF structural analyses show that the hydrogen modes are excited concurrently with the carbon modes. From bond dissociation energies alone, one would expect C-C bonds ($D_{0,\text{expt}} = 83$ kcal/mol) to break more readily than C-H bonds ($D_{0,\text{expt}} = 98$ kcal/mol). eFF overestimates the strength of carbon-carbon σ bonds (for ethane, the bond dissociation energy is 140 kcal/mol versus 110 kcal/mol zero-point energy-corrected snap bond energy).[8] The loss of order in the C-H and H-H RDF functions indicates significant excitation in the hydrogen modes. Likewise, the C-C RDF functions are excited, but for DFT/AM05 and eFF the nearest-neighbor peaks are well defined up to 2.6 g/cm^3. We believe that an entropic effect is the cause of this phenomenon. Carbon atoms are constrained to the polymer backbone by two heavy atoms while hydrogen atoms are only bound to a single heavy atom. This effectively reduces the vibrational flexibility of carbon atoms to pseudo-one-dimensional phonon modes while hydrogen atoms are free to pivot and vibrate in any direction. With a larger phase space, the hydrogen atoms have greater entropy, which might decrease the free energy of dissociation. Additionally, hydrogen atoms may be excited by collisions with neighboring polyethylene chains since they are more likely to collide before their carbon backbone.

C. Conductivity

In order to quantify the conductivity of the shocked system, we determined the direct current conductivity using a classical Green-Kubo analysis.[33,34] We determined the electrical conductivity from our NVE Hugoniot states using the Green-Kubo integral of the electric current correlation function:

$$\sigma_{\text{GK}} = \frac{1}{3k_B T V} \int_0^\infty \langle \mathbf{j}(t) \cdot \mathbf{j}(0) \rangle dt, \tag{5}$$

where $\mathbf{j}(t)$ is the electric current flux, and the integral argument corresponds to the electric current velocity correlation, which

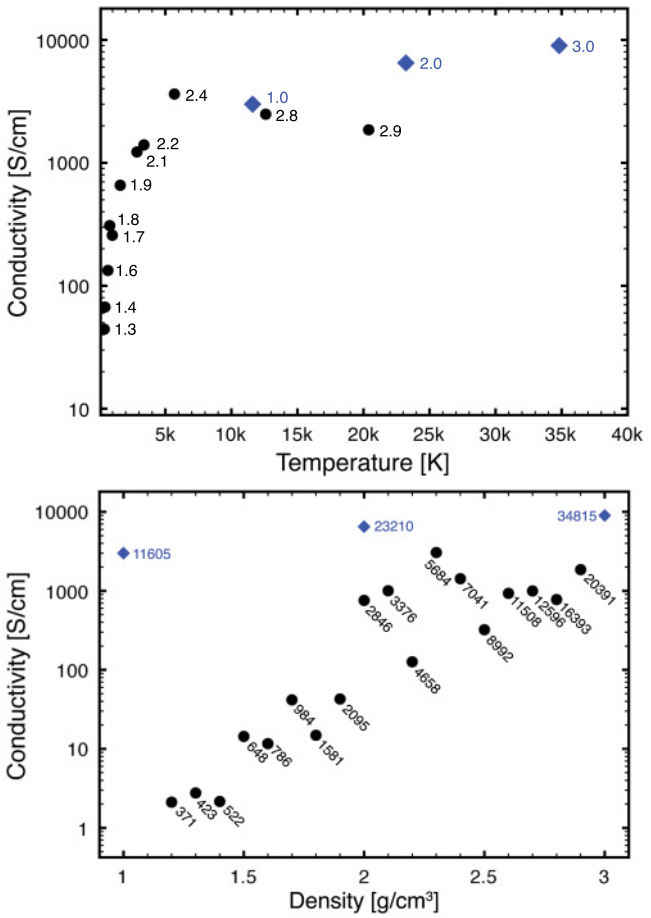

FIG. 5. (Color online) The direct current electrical conductivity of points along the eFF Hugoniot curve (circles) and finite-temperature DFT (diamonds) from Horner.[1] (a) Conductivity plotted against temperature with densities (g/cm^3) provided. (b) Conductivity plotted against density with temperatures (K) provided.

is expressed as

$$J(t) = \langle \mathbf{j}(t) \cdot \mathbf{j}(0) \rangle = \sum_{i=1}^{N} \sum_{j=1}^{N} \langle q_i q_j \mathbf{v}_i(t) \cdot \mathbf{v}_j(0) \rangle, \tag{6}$$

where i and j are different particles, q is the charge on each particle, and $\mathbf{v}(t)$ is the velocity of each particle. Figure 5 shows the results of this analysis for eFF Hugoniot points. eFF predicts that conductivity increases exponentially along the Hugoniot curve until the temperature reaches roughly 5000 K, at which point it levels off. Indeed, FT-DFT studies of PE in the warm dense matter[1] regime find conductivities between 3000 and 10 000 S/cm for samples at 1 g/cm^3 and 11 605 K to 3 g/cm^3 and 34 815 K. Figure 5(a) shows the temperature dependence of the conductivity. Comparing the eFF and FT-DFT data as a whole, there is a clear transition to a metallic state in the vicinity of 5000 K. The downward slope connecting the density points 2.4, 2.8, and 2.9 reflects the sensitivity of the classical Green-Kubo method to thorough equilibration. Outliers were omitted from Fig. 5(a), but all the data points are provided in Fig. 5(b). Between 5000 and 20 391 K, the sample has a conductivity of 2100 S/cm, which is roughly

equivalent to the conductivity of shocked fluid hydrogen at 140 GPa.[35] Above 2.5 g/cm^3, in the metallic PE regime, the RDF analysis suggests that hydrogen is fluid. This suggests that our conductivity analysis might be applicable to hydrogen-rich fluids at high temperatures and pressures.

The quality of our quasiclassical Green-Kubo analysis is a result of the accuracy of the eFF potential. Despite not being formulated in terms of occupied bands near the Fermi level, eFF produces the correct excitations. The eFF potential is rigorously derived from a solution to Schrödinger's time-dependent equation of motion, which integrates two quantum-derived potential terms and classical electrostatics into its Hamiltonian. In particular, the Pauli function is parametrized based on the orthogonalization of valence bond-type orbitals. When a sample is well described by valence bonding, like polyethylene, eFF will succeed in modeling the potential of each electron. Each electron "feels" the correct potential, thus ionization potentials are accurate for carbon and hydrogen. In extreme conditions, the distribution of valence and core electronic states spreads and eventually the highest energy electrons become unbound much like the tail of a Fermi-Dirac distribution above the Fermi level. This behavior explains why we observe the correct carrier mobilities, ionization yields, and conductivities for eFF simulations in extreme conditions.

V. CONCLUSIONS

We have simulated the response of PE to hydrostatic shock compression using the eFF wave-packet molecular-dynamics method. eFF accurately reproduces previously published experimental and theoretical findings for high-energy shock Hugoniots of PE and provides further insight into the effects of electron excitations and ionization at extreme pressures and temperatures (e.g., above 2.4 g/cm^3 the polymer backbone begins to break and electrons begin to ionize, which increases with temperature along the Hugoniot). We find that by 300 GPa, significant structural deterioration and ionization occur. eFF also enabled us to study the electronic conductivity of PE as it transitions at high temperatures into a plasma phase, a unique feature that is impossible to obtain via conventional force fields or BOQMD. The fidelity of the eFF Hugoniot indicates that van der Waals interactions are not important under extreme shock conditions. We expect that the results presented in this paper will stimulate further work on the applicability of eFF to open problems in high-energy–density physics.

ACKNOWLEDGMENTS

This material is based upon work supported by the Department of Energy National Nuclear Security Administration under Award Number DE-FC52-08NA28613 (Caltech PSAAP). P.T. would like to thank John Aidun, Aidan Thompson, and Thomas Mattsson for hosting him at Sandia National Laboratories, where part of this work was initiated. Sandia National Laboratories is a multiprogram laboratory managed and operated by Sandia Corporation, a wholly owned subsidiary of Lockheed Martin Corporation, for the US Department of Energy's National Nuclear Security Administration under Contract No. DE-AC04-94AL85000.

*ajaramil@caltech.edu
†wag@wag.caltech.edu

[1] D. A. Horner, J. D. Kress, and L. A. Collins, Phys. Rev. B **81**, 214301 (2010).
[2] T. C. Sangster, R. Betti, R. S. Craxton, J. A. Delettrez, D. H. Edgell, L. M. Elasky, V. Y. Glebov, V. N. Goncharov, D. R. Harding, D. Jacobs-Perkins, R. Janezic, R. L. Keck, J. P. Knauer, S. J. Loucks, L. D. Lund, F. J. Marshall, R. L. McCrory, P. W. McKenty, D. D. Meyerhofer, P. B. Radha, S. P. Regan, W. Seka, W. T. Shmayda, S. Skupsky, V. A. Smalyuk, J. M. Soures, C. Stoeckl, B. Yaakobi, J. A. Frenje, C. K. Li, R. D. Petrasso, F. H. Sguin, J. D. Moody, J. A. Atherton, B. D. MacGowan, J. D. Kilkenny, T. P. Bernat, and D. S. Montgomery, Phys. Plasmas **14**, 058101 (2007).
[3] P. Amendt, C. Cerjan, A. Hamza, D. E. Hinkel, J. L. Milovich, and H. F. Robey, Phys. Plasmas **14**, 056312 (2007).
[4] T. R. Mattsson, J. M. Lane, K. R. Cochrane, M. P. Desjarlais, A. P. Thompson, F. Pierce, and G. S. Grest, Phys. Rev. B **81**, 054103 (2010).
[5] S. Pittalis, C. R. Proetto, A. Floris, A. Sanna, C. Bersier, K. Burke, and E. K. U. Gross, Phys. Rev. Lett. **107**, 163001 (2011).
[6] N. D. Mermin, Phys. Rev. **137**, A1441 (1965).
[7] R. Car and M. Parrinello, Phys. Rev. Lett. **55**, 2471 (1985).
[8] J. T. Su, Ph.D. thesis, California Institute of Technology, Pasadena, CA (2007) .
[9] J. T. Su and W. Goddard III, Proc. Natl. Acad. Sci. USA **106**, 1001 (2009).
[10] J. T. Su and W. A. Goddard III, Phys. Rev. Lett. **99**, 185003 (2007).
[11] H. Kim, J. T. Su, and W. A. Goddard III, Proc. Natl. Acad. Sci. USA **108**, 15101 (2011).
[12] A. Jaramillo-Botero, J. T. Su, A. Qi, and W. A. Goddard III, J. Comp. Chem. **32**, 497 (2010).
[13] P. L. Theofanis, A. Jaramillo-Botero, W. A. Goddard, III, and H. Xiao, Phys. Rev. Lett. **108**, 045501 (2012).
[14] A. A. Frost, J. Chem. Phys. **47**, 3707 (1967).
[15] C. W. Wilson and W. A. Goddard III, Chem. Phys. Lett. **5**, 45 (1970).
[16] E. J. Heller, J. Chem. Phys. **62**, 1544 (1975).
[17] S. J. Plimpton, J. Comp. Phys. **117**, 1 (1995).
[18] S. J. Plimpton, [http://lammps.sandia.gov/bench.html].
[19] M. J. Doyle, Polym. Eng. Sci. **40**, 330 (2000).
[20] N. K. Bourne, J. C. F. Millett, and S. G. Goveas, J. Phys. D **40**, 5714 (2007).
[21] W. J. M. Rankine, Philos. Trans. R. Soc. **160**, 277 (1870).
[22] H. Hugoniot, J. de l'Ecole Polytech. **57**, 3 (1887) .
[23] M. B. Boslough and J. R. Asay, in *High-Pressure Shock Compression of Solids*, edited by J. R. Asay and M. Shahinpoor (Springer-Verlag, New York, 1993), p. 7.

[24]*LASL Shock Handbook*, edited by S.P. March (University of California Press, Berkeley, CA, 1980) .
[25]W. Nellis, F. Ree, R. Trainor, A. Mitchell, and M. Boslough, J. Chem. Phys. **80**, 2789 (1984).
[26]J. D. Kress, S. R. Bickham, L. A. Collins, B. L. Holian, and S. Goedecker, in *Shock Compression of Condensed Matter*, edited by M. D. Furnish, L. Chhabildas, and R. A. Graham, AIP Conf. Proc. No. 505 (AIP, New York, 2000), p. 381.
[27]R. Armiento and A. E. Mattsson, Phys. Rev. B **72**, 085108 (2005).
[28]S. J. Stuart, A. B. Tutein, and J. A. Harrison, J. Chem. Phys. **112**, 6472 (2000).
[29]W. L. Jorgensen, D. S. Maxwell, and J. Tirado-Rives, J. Am. Chem. Soc. **118**, 11225 (1996).
[30]O. Borodin, G. D. Smith, and D. Bedrov, J. Phys. Chem. B **110**, 6279 (2006).
[31]See Supplemental Material at http://link.aps.org/supplemental/10.1103/PhysRevB.85.094109 for coordination number plots corresponding to the radial distribution functions provided in this paper.
[32]T. R. Mattsson and K. R. Cochrane (private communication).
[33]Y. Shim and H. J. Kim, J. Phys. Chem. B **112**, 11028 (2008).
[34]M. H. Kowsari, S. Alavi, B. Najafi, K. Gholizadeh, E. Dehghanpisheh, and F. Ranjbar, Phys. Chem. Chem. Phys. **13**, 8826 (2011).
[35]W. J. Nellis, S. T. Weir, and A. C. Mitchell, Phys. Rev. B **59**, 3434 (1999).